# A promising method for promoting interfacial adhesion of aramid/rubber composite using atmospheric pressure plasma surface modification

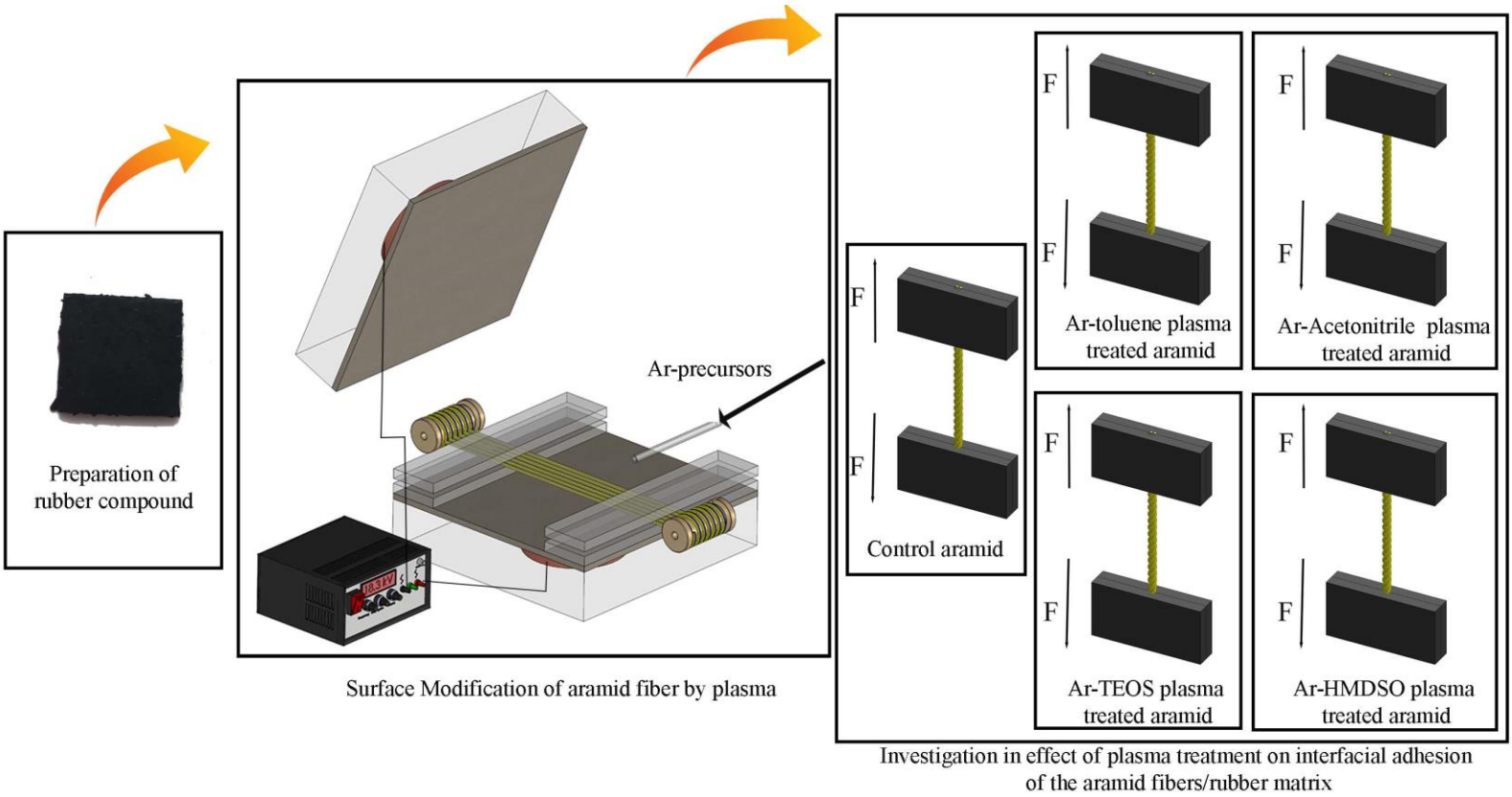


Graphical Abstract

# A promising method for promoting interfacial adhesion of aramid/rubber composite using atmospheric pressure plasma surface modification

Ehsan Shakerinasab[1*], Ensieh Poshtkouhian Bavi[2], Cristina Balagna[3], Monica Ferraris[3]

1. Department of Atomic and Molecular Physics, Faculty of Science, University of Mazandaran, Babolsar, Iran

2. Department of Physics, University of North Texas, Denton, Texas 76203, USA

3. Department of Applied Science and Technology, Politecnico di Torino, Corso Duca degli, Abruzzi 24, Turin, Italy

*** Corresponding Author:** E.Shn1400@gmail.com

## Abstract

Today, aramid fibers are well known as a high-performance and ideal material for reinforcement purposes in rubber product manufacturing including hoses, tires, cables, and conveyors composites. However, surface modification of aramid fiber is necessary to solve poor interfacial adhesion between aramid fibers and the rubber matrix. Accordingly, in the present study, the effect of the surface modification of aramid fibers using atmospheric pressure plasma treatment with different precursors on adhesion to the rubber matrix was investigated. For that, the plasma coating was conducted using argon as the main working gas, and toluene, acetonitrile, tetraethyl orthosilicate (TEOS), and hexamethyldisiloxane (HMDSO) as liquid precursors. The physical-chemical characterization of the layer confirmed the successful deposition of amorphous carbon, amorphous nitride-carbon, $SiO_2$, and Polydimethylsiloxane (PDMS)-like coating layers on the surface of aramid fibers by using toluene, acetonitrile, TEOS, and HMDSO as precursors respectively. Overall, the result showed that the plasma surface modifications with acetonitrile precursor leads to the increase in interfacial adhesion of aramid/rubber composite, while retaining the tensile strength, and flame resistance properties of aramid as original fibers. Notably, the results of this study confirm the potential use of atmospheric pressure plasma for surface modification of aramid yarn to produce functional aramid for use in rubber composites.

**Keywords:** aramid fiber, rubber matrix, composites, plasma

## Highlights

- The plasma-coated aramid using HMDSO, TEOS, toluene, and acetonitrile precursors was prepared, and its effect on the tensile properties of aramid fiber as well as interfacial adhesion between aramid/rubber composite was investigated.
- The positive effect of atmospheric pressure plasma coating using HMDSO precursor on the tensile properties of aramid fiber was revealed.
- The positive effect of atmospheric pressure plasma coating using toluene and acetonitrile on the interfacial adhesion between aramid/rubber composite was revealed.
- The positive effect of atmospheric pressure plasma coating using TEOS precursor on the flam resistance property of aramid fiber was revealed.
- This study provides valuable insights into the effect of the different plasma-coated organosilicon and hydrocarbon precursors on the interfacial adhesion between aramid/rubber composite.

## 1. Introduction

Nowadays, aramid fibers are well known as a high-performance material in various fields and industries, because of their promising properties including high mechanical strength, flame resistance properties, high tenacity, lightweight, and so on. Also in the composite field, aramid fiber is well known as reinforcement material for production of high-performance composites

One of the important reinforcement applications of aramid fibers in high-performance composites productions is for rubber products manufacturing including hoses, tires, cables, and conveyors in the rubber manufacturing industry. This is because of the light weight of the aramid fibers followed by high specific strength, high specific modulus, and low density [1].

However, the poor compatibility between aramid fibers and rubber matrixes, which is due to the chemical inertness, high crystallinity, and high smooth surface properties of aramid fibers restricted its application in the rubber industry. Thus, currently, the whole potential of the aramid fiber is not yet utilized [2-4].

Different surface modification techniques have been developed to promote the adhesion between aramid fiber and rubber matrix [5-11]. These methods include the coating method[12], chemical grafting[13], surface construction of nanostructures[14-16], and plasma treatment[17-19]. The purpose of all of them is to increase the surface roughness and improve the surface chemical activity, which will result in excellent mechanical interlocking and chemical bonding between aramid fiber and matrix [20]. *Zhang et al*. investigate the effects of the surface coating of aramid fiber with graphene/aramid to enhance interfacial adhesion to rubber matrix. The results of this study show the enhancement in interfacial adhesion of aramid fibers to rubber composite followed by maintaining the mechanical properties [2]. *Yang et al.* investigate the effect of the grafting hyperbranched polysiloxane of aramid fibers in increase adhesion to rubber matrix. The results show that this surface modification method can increase the interfacial adhesion of aramid fibers to rubbers matrix [6].

Among the different methods for surface modification of aramid fiber to improve its surface activity, the atmospheric pressure plasma is a known as a promising powerful approach [21, 22]. The process is single-step, cost-effective, simple, and environmentally friendly that can be operated at room temperature. Non-thermal plasma processing is a dry approach that does not require large quantities of toxic chemical materials and water during the treatment process. Also, the process is a surface modification approach. It means that, by the plasma processing, only the surface properties of the samples are treated while bulk properties remain unchanged [23, 24]. So, the plasma processing can be used as a powerful approach for surface modification of aramid fiber to enhance interfacial adhesion of fibers to rubber matrix for composite production. However, the potential use of plasma processing for surface modification of aramid for rubber composite application was rarely investigated. Also, the effect of atmospheric pressure plasma coating on interfacial adhesion of aramid/rubber composite is not investigated before.

In the current study, we investigated the effect of the atmospheric pressure plasma coating with different precursors for surface modification of aramid fiber to increase the adhesion to rubber matrix. More precisely, in the first step, conventional atmospheric pressure dielectric barrier discharge (DBD) plasma with argon as the working gas and four different liquid precursors were used to surface modification of aramid fibers. In the second step, a rubber matrix with pre-defined precursors was fabricated. In the final step, a rubber matrix aramid composite was fabricated and

the effect of the plasma surface modification of aramid fiber on adhesion to aramid to rubber matrix was investigated.

Besides, the effect of the plasma treatment with different precursors on the formation of different chemical structures on the surface of aramid yarn was fully investigated. Regarding results about the plasma treatment of aramid fibers by different precursors, different surface chemical structures form on the surface of aramid fibers that induce different functionality to it. Overall, this process can improve the mechanical strength and of the fibers. Moreover, based on the achieved results, the plasma surface modification of aramid fibers can lead to the adhesion of aramid fiber to rubber matrix. This makes it suitable for reinforcement and flame resistance applications in different industries.

In summary, in this study, the application and advantage of using atmospheric pressure DBD plasma for surface modification of aramid fibers for rubber application was investigated and proved. The results promise the use of atmospheric pressure plasma for textile industries and joining application.

## 2. Materials and Methods

### 2.1 Plasma surface coating on aramid fiber

In this work, a conventional atmospheric pressure dielectric barrier discharge (DBD) plasma was employed as a plasma source for the surface treatment of aramid fibers. The upper and lower electrodes of the DBD system are cylindrical with a diameter of 5 cm, and both of its covered with 0.5 mm thickness PTFE dielectric. Also, the ignition gap is fixed at 4 mm.

An argon gas with a purity of 99.9 was used as the feed gas for the ignition of the plasma. The feed gas goes through liquid precursors, during its pass to the ignition gap, including tetraethyl orthosilicate (TEOS), hexamethyldisiloxane (HMDSO), toluene, and acetonitrile to insert organosilicon and hydrocarbon precursors into the system.

For the treatment of aramid fibers, the fiber was inserted between the two electrodes by winding the device at an adjustable speed, and exited from the other sides. The plasma conditions and experimental parameters for the treatment of the fibers are listed in the Table1.

It should be noted that, before the treatment, the substrates were ultrasonically cleaned with acetone 99%, ethanol 99%, and deionized water respectively, each one for 10 min, and dried under atmospheric pressure.

**Table1.** Plasma deposition condition on aramid fiber

| Sample name | Deposition time (min) | Ar flow rate ($\frac{L}{min}$) | Plasma power (W) |
|---|---|---|---|
| Pristine aramid fiber | 10 | 1.5 | 26 |
| Ar/TEOS coated aramid fiber | 10 | 1.5 | 26 |
| Ar/HMDSO coated aramid fiber | 10 | 1.5 | 26 |
| Ar/toluene coated aramid fiber | 10 | 1.5 | 26 |
| A/acetonitrile coated aramid fiber | 10 | 1.5 | 26 |

### 2.2 Preparation of aramid/rubber composite

The rubber compounds were prepared by mixing the ingredients according to the rubber formula detailed in Table 1 in an internal mixer device (50 cc, Brabender, Germany). For this purpose, in the first step Styrene Butadiene Rubber 1520 and Standard 10 Malaysian rubber were mixed for 1 min in an internal mixer. In step two, Antioxidant 4020 (6PPD), zinc oxide, coumarone indene resin, stearic acid, Adhesive (RS) and Accelerant (CZ) were mixed for 5 min; in step three, carbon black, white carbon black and Aromatic oil 840 were added to mix for 3 min; and finally, in step four, sulphur and rubber adhesive (RA) were mixed for 1 min. All the tests were performed at 80 C.

After the preparations of the rubber composite, the mixture is compressed into rubber sheets with a 5 mm diameter by two roll mills. Afterward, two sheets were placed in the mold and the aramid was embedded between them. The mold was pressed at 140 °C for 45 min under 20 MP pressure. The process is schematically presented in Fig 1a.

**Table 2.** the rubber compounding materials

| | Ingredients | Parts per hundreds of rubbers (Pehr) |
|---|---|---|
| 1 | Styrene Butadiene Rubber 1520 | 70 |
| 2 | Standard 10 Malaysian rubber | 30 |
| 3 | Carbon black N330 | 25 |

| | | |
|---|---|---|
| 4 | Aromatic oil 840 | 10 |
| 5 | White carbon black | 10 |
| 6 | Coumarone-indene resin | 10 |
| 7 | Zinc oxide | 5 |
| 8 | Antioxidant 4020(6PPD) | 4 |
| 9 | Stearic acid | 2 |
| 10 | Accelerant (CZ) | 1.5 |
| 11 | Sulphur | 1 |
| 12 | Adhesive (RA) | 1 |
| 13 | Adhesive (RS) | 1 |
| | Total | 170.5 |

### 2.3 Physical and Chemical Characterizations

First, the morphological characterization of the sample was performed by Field-emission scanning electron microscopy (FE-SEM) method. The test was assessed by a ZEISS Field Emission SEM device equipped with dispersive X-ray spectroscopy (EDS) and Map analysis.

Then, the chemical characterization was performed by Fourier transforms infrared (FTIR), Raman spectroscopy, X-ray diffraction (XRD) analysis, and X-ray photoelectron spectroscopy (XPS). The FTIR analysis was performed using the attenuated total reflectance (ATR) mode of Thermo-Nicolet Avatar 380 FTIR spectrometer in the range of 4000-600cm-1. XRD analysis was conducted using Philips PW1730 an X-ray diffractometer in the range of 10-85 $^{o}$C with the step of 0.05 $^{o}$/s. We used the radiation source of Cu Kα in 1.542 Å wavelength. The Raman spectra were performed by TakRam N1-Raman analyzer in 532 nm excitation wavelength. XPS analysis was conducted by Phi 5000 Versa ProbeTM XPS device.

Finally, thermal analysis was performed by Thermo-gravimetric analysis (TGA). TGA was performed to investigate the thermal decomposition of the uncoated and plasma-coated aramid fiber using NETZSCH's STA 2500 instrument. The temperature range was 30–800 °C and the heating rate was 10 °C/min. The experiment was carried out in the ambient atmosphere.

### 2.4 Mechanical Performance

The effect of the plasma surface coating by different precursors on the mechanical performance of aramid fiber was investigated using a breaking strength test. For that, a Micro 350, Shirley universal testing machine with a gauge length of 500 mm was conducted.

Before the test, a TSH006 TST counts denier textile reeling length measuring instrument was used to measure the denier of the fibers. The specific stress was calculated by converting the denier unit to tex and using the equation below.

$$\text{Specific Stress (Force per unit linear density)} = \frac{\text{Maximum force required for fiber breakdowns}}{\text{fiber tex}} \left(\frac{\text{N}}{\text{tex}}\right)$$

Denier = Weight per gram of 9000 meter or 9 km of yarn

Tex = Weight per gram of 1000 meter or 1 km of yarn

Finally, the specific stress versus strain diagram was used for comparing uncoated and plasma-coated aramid fiber by different precursors.

### 2.5 Pull out test

The interfacial adhesion of aramid yarn to rubber matrix was investigated by the pull-out test. For this purpose, the pull-out test was conducted on previously produced aramid/rubber composite. we used of Shirley micro X350 universal testing machine with an adjusted speed of 3 mm per minute. The process is schematically displayed in Fig 1b. The analysis was performed on 10 repeats to ensure accuracy, and the average amount of maximum pull-out force was calculated.

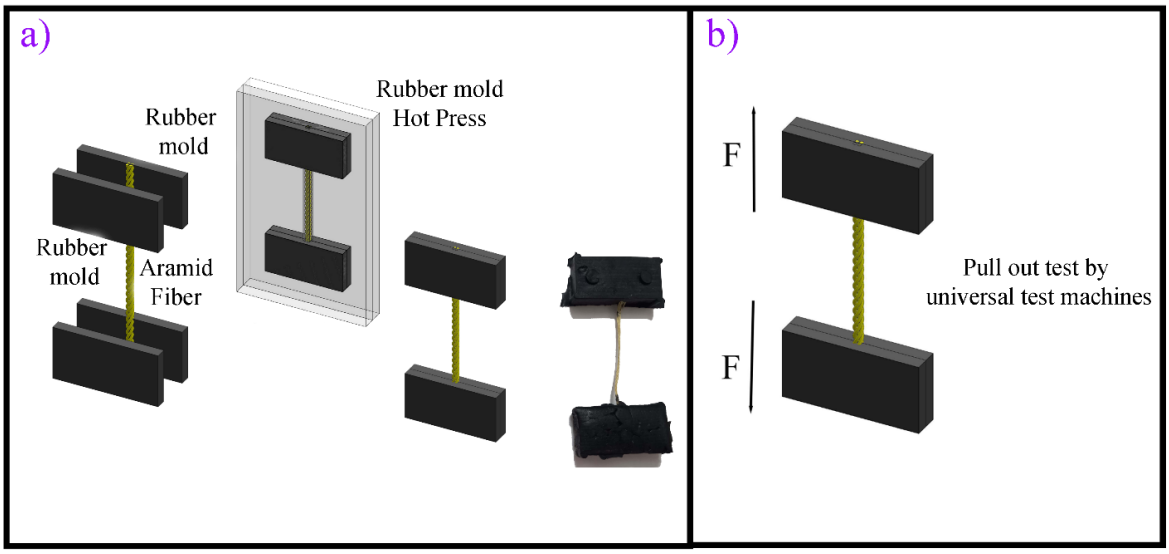


**Fig 1.** a) schematics of the process for aramid rubber compound production b) Structure of pull-out test

## 3. Results and discussions

### 3.1 Structural characterization

Fig 2 shows the FESEM images of uncoated and plasma-coated aramid fibers. As can be seen in the figure, the uncoated aramid fibers show a completely smooth surface without any striations

and longitudinal markings on its surface. In contrast, plasma surface coated aramid fiber by different precursors shows completely different structures. Based on the results, the plasma treatment with different precursors lead to the formation of nanostructures with different configurations on the surface of the aramid.

Also, based on the results, a nano-sphere particle layer entirely covered the surfaces of the aramid by plasma surface coating with hydrocarbon precursors, while, the treatments by organosilicon precursors lead to forming a thick nearly smooth layer on the surfaces. However, the diameter of the nanosphere formed on the surface of toluene-coated aramid is very higher than that of acetonitrile-coated fiber. The first is at around 100 nm and the second at 2 μm. This result is may be related to the easier degradation of toluene in plasma[25].

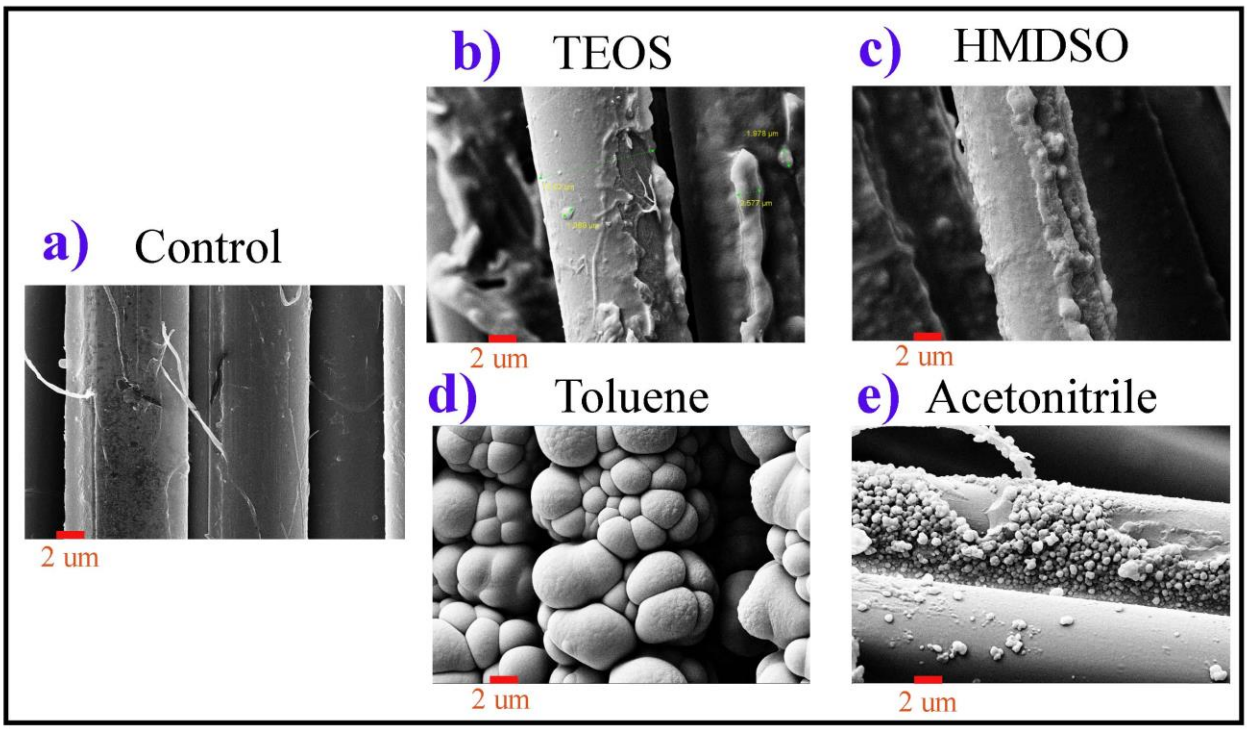


**Fig 2.** FESEM images of a) uncoated and plasma-coated aramid fiber using b) TEOS c) HMDSO d) toluene e) Acetonitrile precursors at 2μm magnification

### 3.2 Chemical structures and compositions

The ATR-FTIR analysis was employed to measure the changes in chemical structure of aramid fiber after the plasma coating (Fig. 3). It should be noted that, all spectra normalized based on the band at 820 $cm^{-1}$. This bond is related to out-of-plane bending of the C-H of aromatic ring in the backbone structure of the aramid fiber, which is a main characteristic peak of the aramid. Also,

the intensity of this peak does not have considerable variations upon the treatment of the aramid fiber [26].

The full-length spectrum of uncoated and plasma coated aramid fibers using toluene, and acetonitrile precursors displayed in Fig 3a. As can be seen in this figure, these samples display similar spectra and similar bonds comparing to uncoated aramid fibers. The main chemical bond of uncoated aramid fiber is listed in Table 3. This bands are included the aromatic C-H out of plane bends, -C-N stretching (primary amine), -NH- and C-C vibration, Amide III (C-N stretching, -NH- bending), C-C vibrational in benzene skeleton, Amid II (C-N stretching, N-H bending), amide I band (C=O Stretching), C-H stretching, amid A (N-H stretching) and N-H stretching at 818, 1103, 1249, 1300, 1388, 1505, 1536, 1640, 2846, 2915, 2958, and 3305 $cm^{-1}$, respectively [8, 27]. However, based on the plasma treatment with different precursors, some changes happened in band intensity and position and some new chemical bonds appeared.

Fig. 3b, c shows the FTIR spectrum of uncoated and plasma-coated aramid fiber by toluene and acetonitrile precursors, respectively. As can be seen from the results, after the plasma depositions by toluene precursors, one shoulder peak was added at the position of 1608 $cm^{-1}$ as depicted in Fig 3b. This peak is related to C=C stretching groups. Also, the peaks at 1504 $cm^{-1}$ and 1535 $cm^{-1}$ grew upon the plasma treatments by toluene precursors which indicates the formation of C-H stretching bonds on the surface of the aramid yarns. The results indicate in deposition of amorphous carbon-containing groups on the surface of aramid fibers [28, 29].

Also, based on plasma treatment by acetonitrile precursors, one broad peak with high intensity appeared between 2200 to 2400 $cm^{-1}$ with a center of 2179 $cm^{-1}$ as depicted in Fig. 3c. This peak is characteristic of the C=N stretching mode bond, which arises from the electron decomposition of acetonitrile in plasma and deposition of the C=N group. The results indicated in the deposition of amorphous carbon nitride groups on the surface of aramid fibers [30-33].

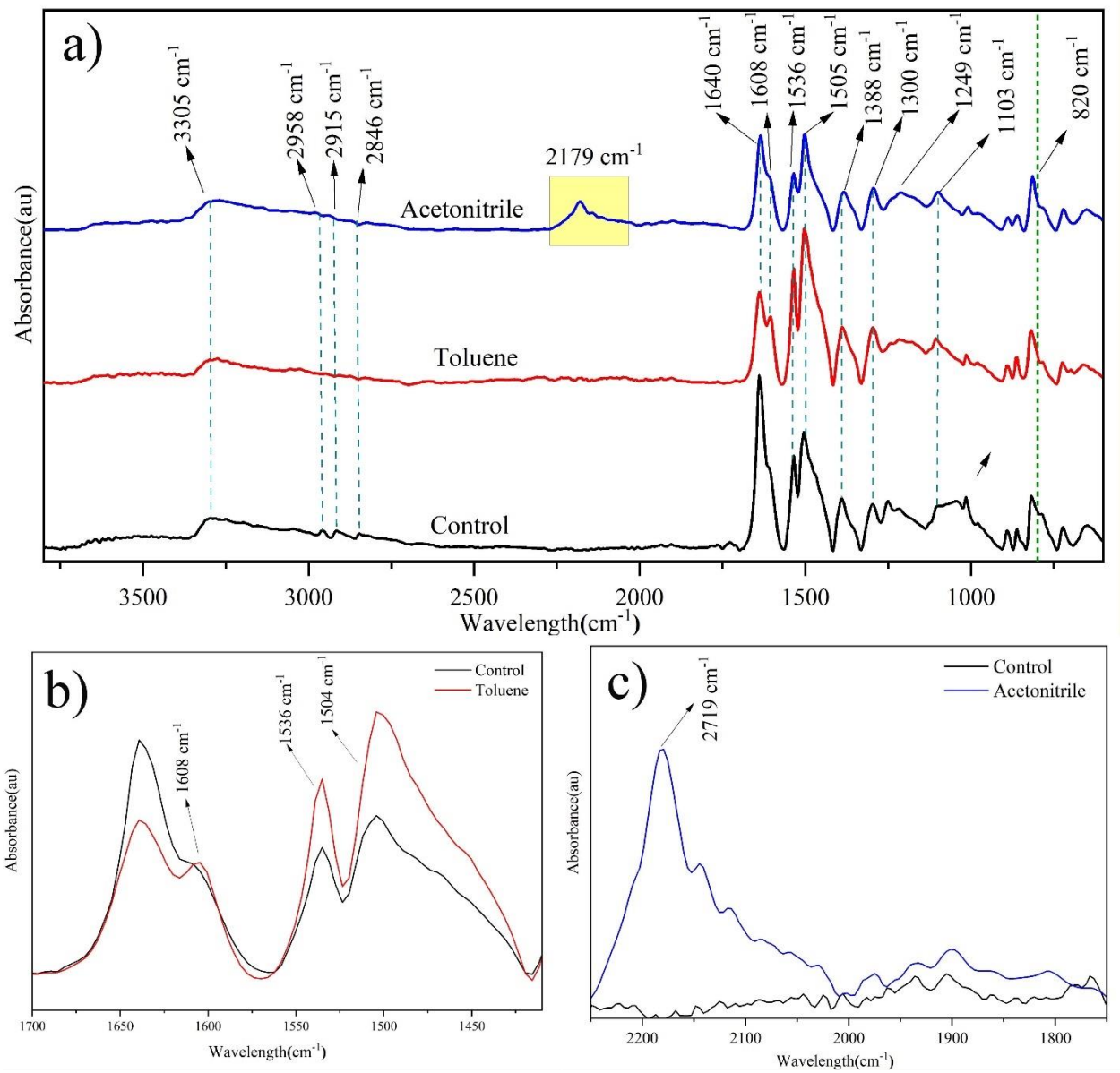


**Fig 3.** (a) Full-range FTIR spectra of the uncoated and plasma-coated aramid fiber with toluene and acetonitrile precursors (b) overlay view of plasma coated sample with toluene precursor within the ranges of 1420 to 1700 $cm^{-1}$, (c) overlay view of plasma coated sample with acetonitrile precursor within the ranges of 1720 to 2250 $cm^{-1}$

**Table 3.** The FTIR chemical band of the uncoated and plasma-coated aramid fiber [8, 27]

| Wavelength ($cm^{-1}$) | Assignments |
|---|---|
| 818 | Aromatic C-H out of plan bends |
| 1103 | -C-N stretching (primary amine), -NH- and C-C vibration |

| | |
|---|---|
| 1249 | Amide III (C-N stretching, -NH- bending) |
| 1300 | |
| 1388 | C-C vibrational in benzene skeleton |
| 1505 | |
| 1536 | Amid II (C-N stretching, N-H bending) |
| 1640 | Amide I band (C=O Stretching) |
| 2846 | C-H stretching |
| 2915 | |
| 2958 | |
| 3305 | Amid A (N-H stretching) |

Fig 4a shows the FTIR spectrum of uncoated and plasma-coated aramid fiber by TEOS and HMDSO precursors. As can be seen from the results, after the plasma depositions by TEOS precursors, the peak between 830 to 1330 $cm^{-1}$ incrementally grew. These peaks with a center of 1051 $cm^{-1}$ are the characteristic peak of Si-O-Si groups. For further investigation, a Gaussian fit was performed in the range of 830 to 1330 $cm^{-1}$ shown in Fig. 4b. The corresponding peaks were detailed in Table 4. Based on the results, the deconvoluted spectrum contains Si-O asymmetrical bending, Si-$(CH_2)_n$-Si, Si-O asymmetrical stretching, C-O stretching, Si-O asymmetrical stretching, and C-H vibration in $CH_2$ bonds at 859.8, 886.93, 954.53, 1051.7, 1103.3, 1160.7, 1164.81, and 1298.16 $cm^{-1}$, respectively. Also, as can be seen in Fig 4c three peaks at 1454, 1465, and 1481 $cm^{-1}$ appeared which is the characteristic peak of C=C stretching bonds. All the results indicated the formation of a $SiO_2$ layer on the surface of the aramid fibers [32, 34-36].

Finally, plasma coating with HMDSO precursors leads to the intense change in the FTIR spectrum that is indicated in Fig 4d-e. The main changes depicted in Fig 4d plasma coated spectrum with HMDSO precursor included the growth of peak at 1504, and 1535 $cm^{-1}$ related to C-H stretching bonds. Also, one shoulder peak was added at the position of 841 $cm^{-1}$ as depicted in Fig 4b. This peak is related Si-$(CH_3)_3$ groups. The results indicate the formation of SiC film on the surface of aramid fibers by the plasma treatment. [37, 38].

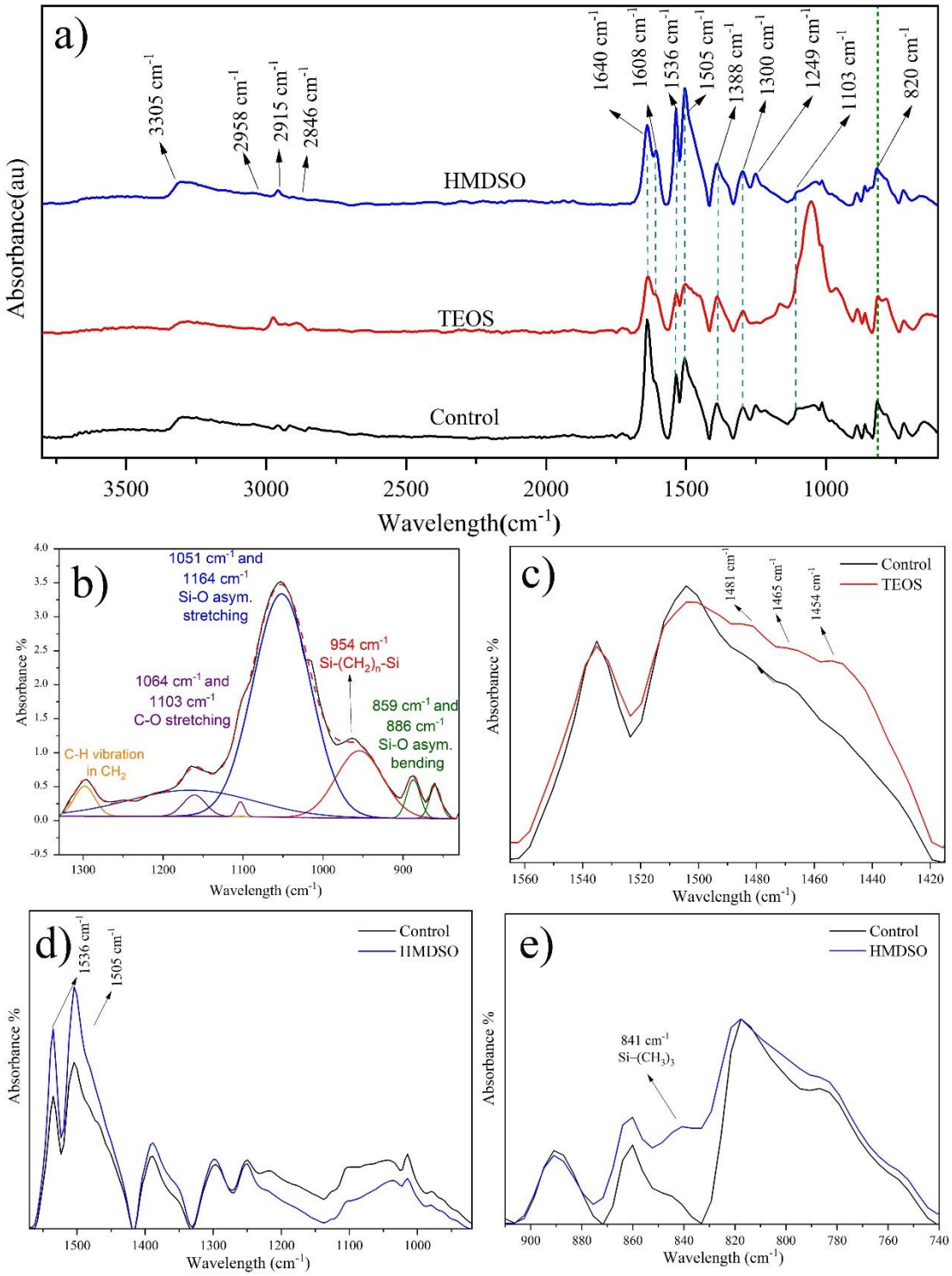


**Fig 4.** (a) Full-range FTIR spectra of the uncoated and plasma-coated aramid fiber with TEOS and HMDSO precursors, overlay view of plasma coated sample with TEOS precursor within the ranges of b) 830 to 1330 $cm^{-1}$ c) 1410 to 1570 $cm^{-1}$., overlay view of plasma coated sample with HMDSO precursor within the ranges of d) 920 to 1570 $cm^{-1}$ e) 740 to 920 $cm^{-1}$

**Table 4.** Peak assignment of Gaussian fitting curves for FTIR spectrum of plasma coated sample with TEOS precursor in the range of 830 to 1330 $cm^{-1}$ [32, 34-36].

| Vibrational mode | Wavenumber ($cm^{-1}$) | Integration area | FWHM | Peak intensity |
|---|---|---|---|---|
| Si-O asymmetrical bending | 859.9 | 8.5 | 16.9 | 0.48 |
| Si-O asymmetrical bending | 886.9 | 12.1 | 20.1 | 0.57 |
| Si-$(CH_2)_n$-Si | 954.5 | 72.8 | 68.9 | 0.99 |
| Si-O asymmetrical stretching | 1051.7 | 294.2 | 84.1 | 3.28 |
| C-O stretching | 1103.4 | 2.7 | 11.6 | 0.22 |
| C-O stretching | 1160.8 | 11.1 | 33.2 | 0.31 |
| Si-O asymmetrical stretching | 1164.8 | 74.4 | 184.8 | 0.38 |
| C-H vibration in $CH_2$ | 1298.2 | 14.1 | 30.3 | 0.44 |

To acquire additional insight into the deposited layer, an XPS analysis was performed on the samples surface. The survey spectrum of the uncoated and plasma-coated aramid fiber is depicted in Fig 5. The results indicate the present of carbon, oxygen, nitrogen, and silicon atoms in different samples whose composition and elemental ratios are presented in Table 5.

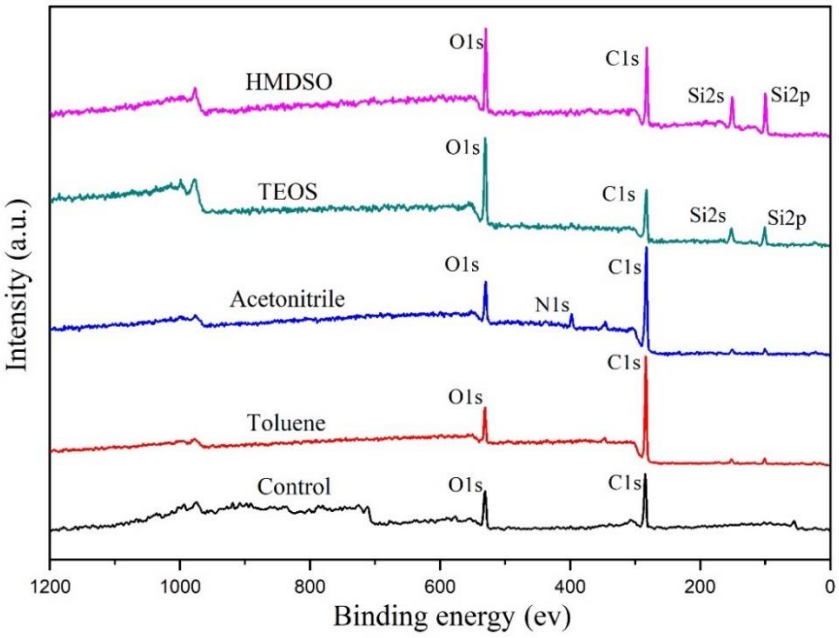


**Fig 5.** XPS survey spectrum of uncoated and plasma coated aramid fiber with different precursors.

**Table 5.** Atomic ratio of the carbon, oxygen, nitrogen, and silicon elements of the uncoated and plasma-coated aramid fiber

| | C (%) | O (%) | N (%) | $Si_2S$ (%) | $Si_2P$ (%) | C/O | C/N | Si/C | Si/O |
|---|---|---|---|---|---|---|---|---|---|
| Control | 57.24 | 38.69 | 4.06 | 0.00 | 0.00 | 1.48 | 14.08 | 0.00 | 0.00 |
| Toluene | 73.96 | 24.41 | 1.63 | 0.00 | 0.00 | 3.03 | 45.37 | 0.00 | 0.00 |
| Acetonitrile | 63.29 | 25.95 | 10.76 | 0.00 | 0.00 | 2.44 | 5.88 | 0.00 | 0.00 |
| TEOS | 45.96 | 28.62 | 4.81 | 9.34 | 11.26 | 1.61 | 9.55 | 0.45 | 0.72 |
| HMDSO | 33.85 | 31.70 | 4.09 | 12.14 | 18.49 | 1.07 | 8.28 | 0.90 | 0.97 |

Comparing the plasma-coated samples with uncoated one for toluene precursors, the plasma deposition with toluene precursors leads to the obvious increase in the C/O and C/N atomic ratio which suggests the formation of a new carbon-containing group on the surface of aramid fibers. For more investigation, a Gaussian fit was performed on the C1s and O1s spectrum of uncoated and plasma-coated aramid fibers depicted in Fig. 6 and 7.

As can be seen from Fig 6a, the C1s curve fitted spectrum of uncoated aramid fibers included the three peaks at 284.97 eV, 286.6 eV, and 288.46 eV which is related to C–C and C=C bonds, C-N bonds, and C-O bonds, respectively. Also, the O1s spectrums depicted in Fig 7, show two characteristic peaks of aramid fibers at 531.23 eV and 532.91 eV that are dedicated to O=C–O and O=C–N structures, respectively [39-42].

Fig 6c and d show the curve-fitted spectrum of plasma-coated aramid fiber by toluene precursor. As can be seen from C1s spectra, after the plasma treatment with toluene precursor one extra peak appeared at 284.55 eV. This peak is mainly related to graphite-like structures. Also, the O1s Spectra of plasma-coated aramid fiber with toluene precursor, similar to the pristine aramid fibers shows the characteristic peaks of 531.17, and 531.79 related to the O=C–O and O=C–N follow decreasing in the intensity of O=C–N peak. The results indicate in deposition of diamond-like carbon coating on the surface of aramid fibers [43-47].

The survey spectrum of plasma-coated aramid fibers with acetonitrile precursor shows an increase in the C/O atomic ratio and a decrease in the C/N atomic ratio which suggest the formation of new carbon nitride on the surface of aramid fibers. Fig 6cand d show the spectrum of plasma-coated aramid fiber by acetonitrile precursor. As can be seen from C1s spectra, similar to the plasma-

292 coated sample with toluene precursors, one extra peak appeared at 284.65 eV which relates to the
293 graphite-like structures induced by plasma deposition. Besides, the results show the increment in
294 C-N, C=N at 286.05 eV, and N-C=O peaks at 288.1 eV. Furthermore, the O1s Specta of plasma-
295 coated aramid fiber with acetonitrile precursor shows the characteristic peaks of 530.60 eV, and
296 532.20 eV related to the O=C–O and O=C–N. The results indicate the deposition of the amorphous
297 nitride carbon layer on the surface of aramid fibers [39, 40, 43].

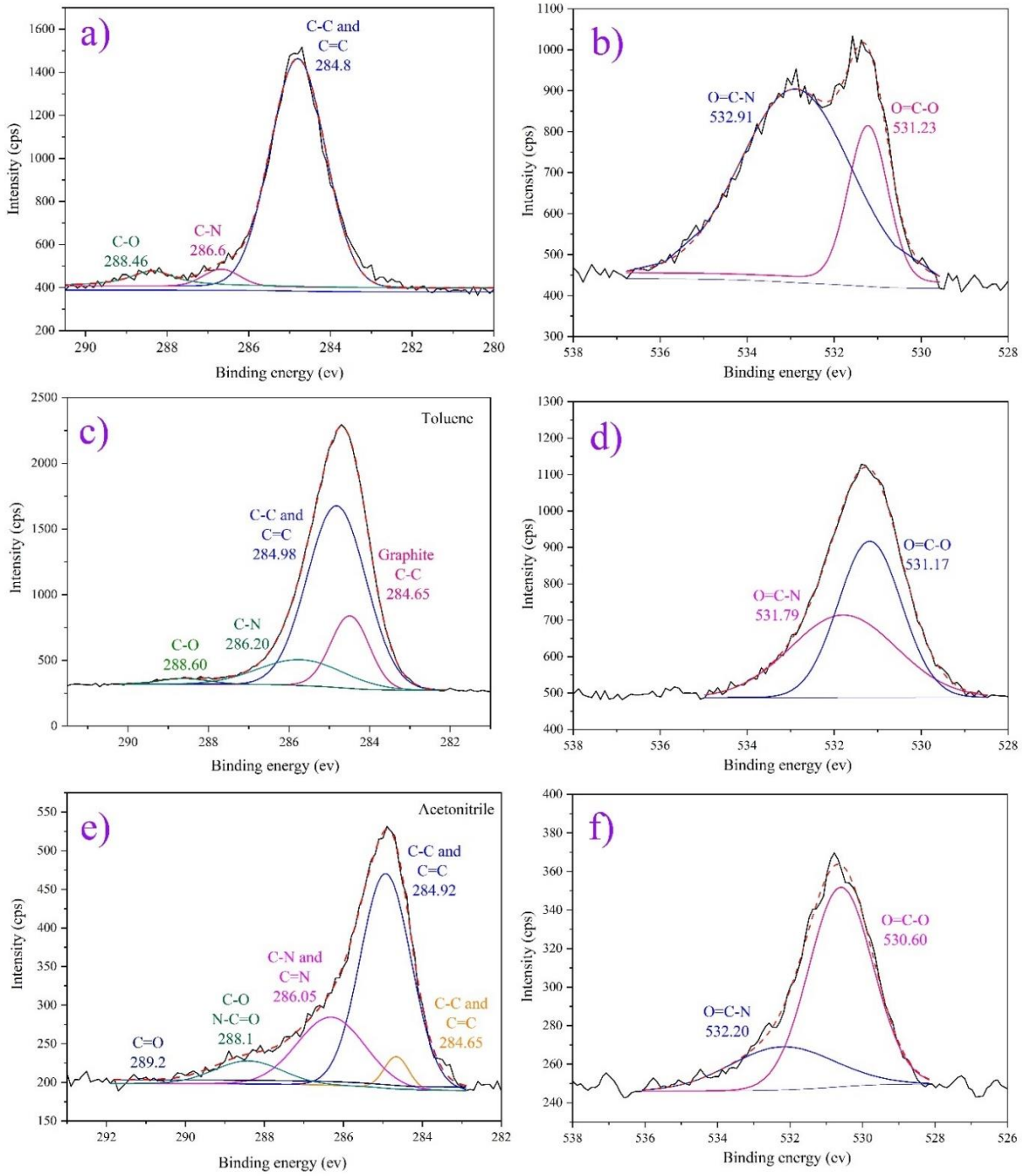


**Fig 6.** Curve fitted spectra for a) C1s spectra of uncoated aramid fiber, b) O1s spectra of uncoated aramid fiber, c) C1s spectra of plasma coated aramid fiber with toluene precursor, d) O1s spectra of plasma coated aramid fiber with toluene precursor, e) C1s spectra of plasma coated aramid fiber with acetonitrile precursor, f) O1s spectra of plasma coated aramid fiber with acetonitrile precursor

The survey spectrum of plasma-coated aramid fibers with TEOS precursors shows the formation of new silicon-containing groups on the surface of aramid fibers. Fig 7a, and 6b shows the curve-fitted spectrum of plasma-coated aramid fiber by TEOS precursor. Based on the results, in the C1s spectrum, we have one increase in the intensity of the peak located at 286.2 eV related to C-O and C-N structures. Furthermore, two new peaks add at the location of 531.59 eV and 534.49 eV related to the Si-O-C and O-C-O groups. the results indicate in the formation of new SiO layers on the surface of aramid fibers [48, 49].

Also, the survey spectrum of plasma-coated aramid fibers with HMDSO precursors shows the formation of new silicon-containing groups on the surface of aramid fibers. Fig 6c, and 6d show the curve fitted spectrum of plasma-coated aramid fiber by HMDSO precursor. As can be seen from C1s, and O1s spectrums, the fitting method consisted of four structures of silicon, including $SiO_2$, $SiO_3(CH_3)$, $SiO_2(CH_3)_2$, and $SiO(CH_3)_3$, as abundantly available in many literatures [35-39] The results indicated fabrication of PDMS like layer on the surface of aramid fiber followed by a crosslinking process of organosilicon polymer chains during plasma coating on the surfaces [50]. All the results of the XPS analysis confirmed the results of FTIR.

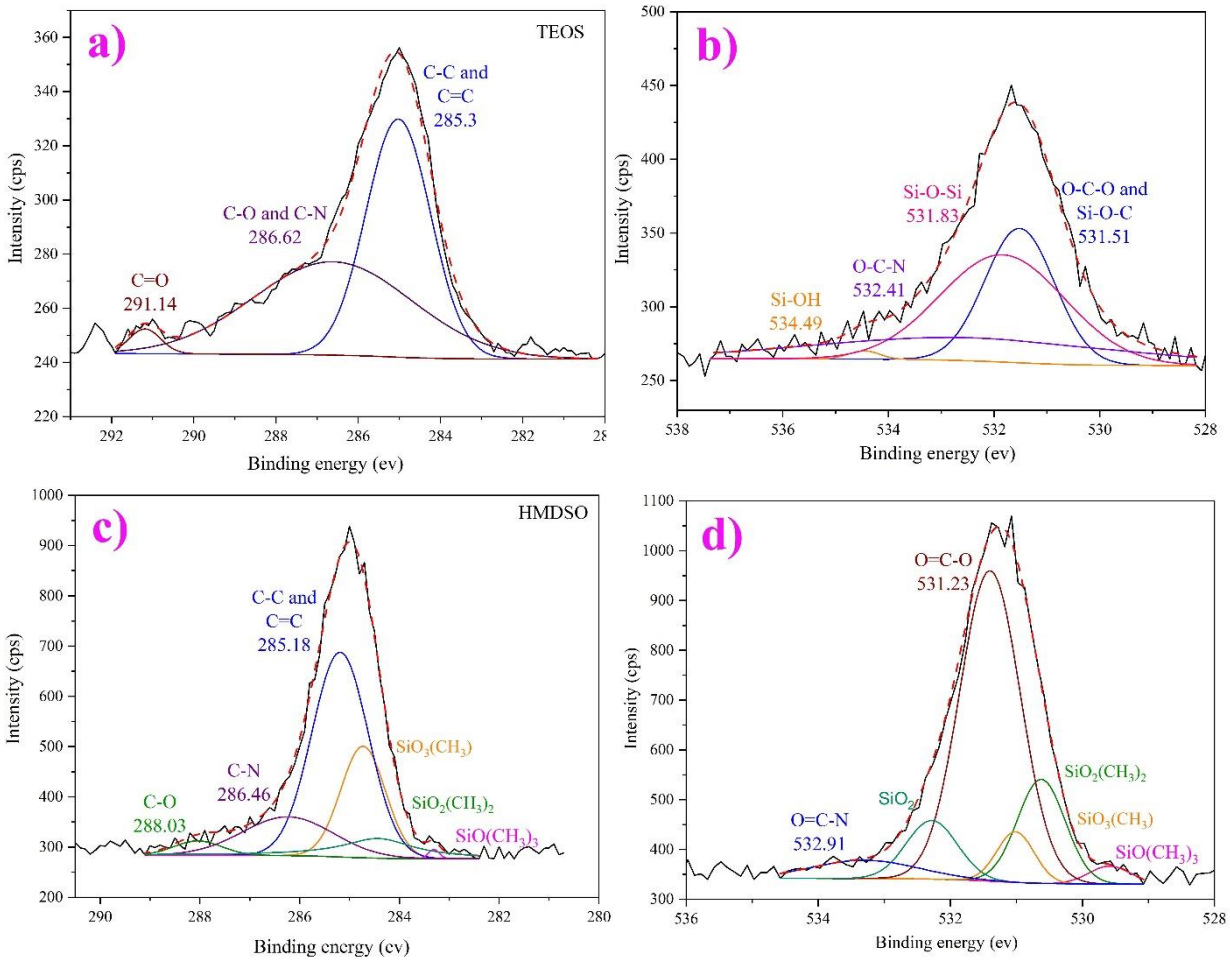


**Fig 7.** Curve fitted spectra for a) C1s spectra of plasma coated aramid fiber with TEOS precursor, b) O1s spectra of plasma coated aramid fiber with TEOS precursor., c) C1s spectra of plasma coated aramid fiber with HMDSO precursor, d) O1s spectra of plasma coated aramid fiber with HMDSO precursor

Further investigation in chemical structures of the sample was investigated by EDS analysis. The results are depicted in Table 6. As can be seen from the results, the plasma coating with toluene precursor leads to the increase in the weight percentage of C element on the surface from 79.3 % to 96.6 %. This shows the good deposition of carbon chemical groups on the surfaces. On contrary, the plasma coating with acetonitrile precursors leads to an increase in nitrogen groups based on the chemical formula and structures of acetonitrile $C_2H_3N$.

For the plasma coating with organosilicon precursors, a new silicon element appeared on the surface of the aramid sample after the plasma treatment which indicated well deposition of a layer on the surfaces. All the results confirmed the FTIR and XPS results.

**Table 6.** weight percentage of the carbon, oxygen, nitrogen, and silicon elements of the uncoated and plasma-coated aramid fiber

| | C (%) | O (%) | N (%) | Si (%) | C/O | C/N | Si/C | Si/O | Si/O |
|---|---|---|---|---|---|---|---|---|---|
| Control | 79.3 | 14.7 | 6 | 0 | 5.39 | 13.22 | 0 | 0 | 0 |
| Toluene | 96.6 | 2.9 | 0.5 | 0 | 33.31 | 193.20 | 0 | 0 | 0 |
| Acetonitrile | 77.9 | 14.4 | 7.7 | 0 | 5.41 | 10.12 | 0 | 0 | 0 |
| TEOS | 69.3 | 16.7 | 8.8 | 5.2 | 4.15 | 7.88 | 0.08 | 0.31 | 0.59 |
| HMDSO | 72.8 | 15 | 7.2 | 5.1 | 4.85 | 10.11 | 0.07 | 0.34 | 0.71 |

The XRD analysis was performed to investigate the effects of the plasma coating with different precursors on the crystal structure of the fiber. The XRD diagram and corresponding fitting curve results of the uncoated and plasma-coated aramid fibers are shown in Fig. 8(a-f).

Based on the results, The aramid fibers exhibited four strong peaks centered at 20.75°, 23.09°, 29.05° and 38.45° associated with the crystal planes (110), (200), (211) and (220) [7, 9-12]. As can be seen from Fig 8a, The XRD patterns of the samples are very similar to each other, this is indicating in the point that no new crystal structure formed on the surface of the aramid fibers after the plasma coating.

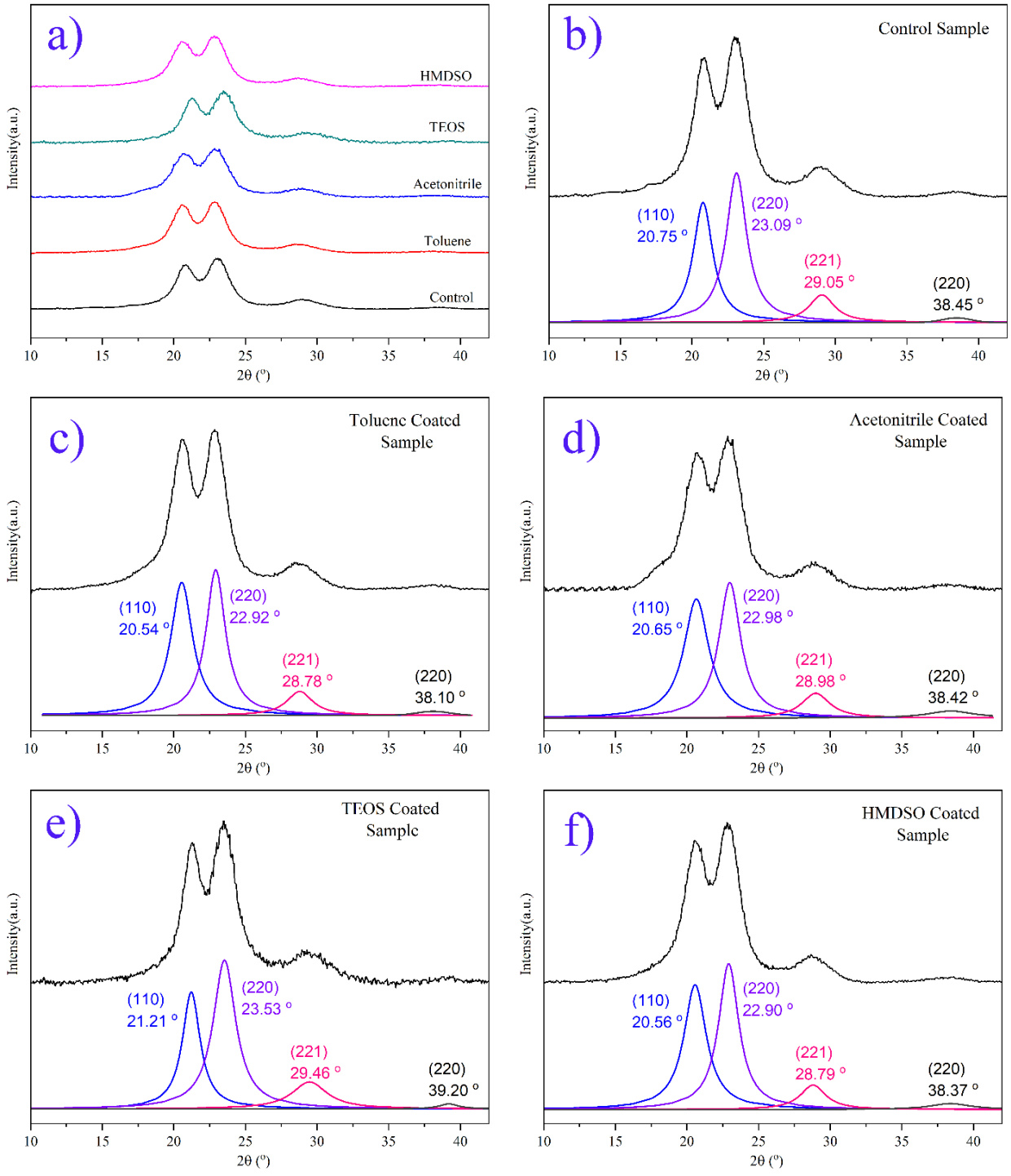


**Fig 8.** a) XRD analysis peaks and corresponding fitting results for b) control sample and the fibers coated with c) toluene d) Acetonitrile e) TEOS f) HMDSO precursors

The crystallite size of two strong peaks of aramid fiber including the (110) and (200) planes for the uncoated and plasma-coated aramid fibers with different precursors depicted in Figure 9a. As

can be seen from the results, the crystallite sizes of the (110) and (200) planes have been decreased with plasma coating with all precursors. These decreases can be related to the inducing defects in the crystal planes as a result of the plasma surface coating on aramid fiber.

Additional investigation into the chemical structures of aramid fiber after plasma coating with different precursors was performed by Raman spectroscopy. The results are depicted in Fig 9b. It should be noted that all the spectrums were baseline corrected and normalized by the band at 1610 $cm^{-1}$. This bond is related to the C-C stretching vibrations which are characteristic of aramid fiber and doesn't main changes base on the fiber treatments. Based on the results, not any difference can be seen in the Raman spectrum of uncoated and plasma-coated aramid fibers with different precursors. This is due to the high level of crystallinity of the aramid fibers that make it difficult to change in the Raman spectrum of aramid fibers.

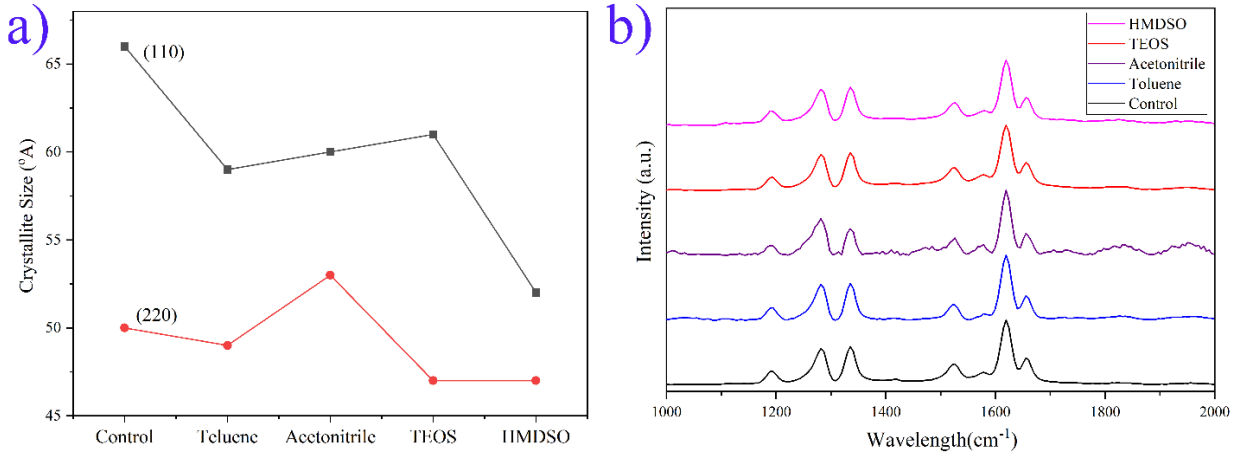


**Fig 9.** a) Crystallite sizes of (110), and (220) plans and Raman spectra of uncoated and plasma-coated sample with different precursors

### 3.3 Thermal Decomposition Analysis

Fig 10 shows the thermal decomposition curves of uncoated and plasma-coated fiber using toluene, acetonitrile, TEOS, and HMDSO precursors. Also, Table 7 detailed the residual percentage of fibers in different temperatures. As can be seen from the table, uncoated aramid fiber shows exhibited a weight loss of 99.77% between 0 and 800°C, which is related to the decomposition of partial dihydroxylation and alkoxide aramid fiber.

Compared with it, the weight loss between 0 to 800 °C for plasma-coated samples with toluene, acetonitrile, TEOS, and HMDSO precursors are 99.00, 99.88, 92.50, and 99.82 % respectively.

The TG curve of plasma-coated samples with HMDSO, and TEOS precursors shows more stability compared to plasma-coated samples with acetonitrile and toluene precursors. For the plasma-coated sample with HMDSO, and acetonitrile precursors, the weight loss in different temperatures was not significantly different with uncoated fiber.

Also, for the plasma-coated sample with TEOS precursor, the weight loss between 0 to 800 °C is 92.50, which is increased by 5.27% compared with the uncoated aramid fiber. Accordingly, it can be said that the plasma-coated sample with TEOS precursors has a positive effect on the thermal decomposition of aramid fiber.

However, based on the results, the plasma coating with hydrocarbon precursors including toluene and acetonitrile led to more weight loss in the range of 0 to 800 °C. The reason is may due to the more thermal stability of Si-O-Si bonds compared to C-C, C-N, and C-O [6, 51].

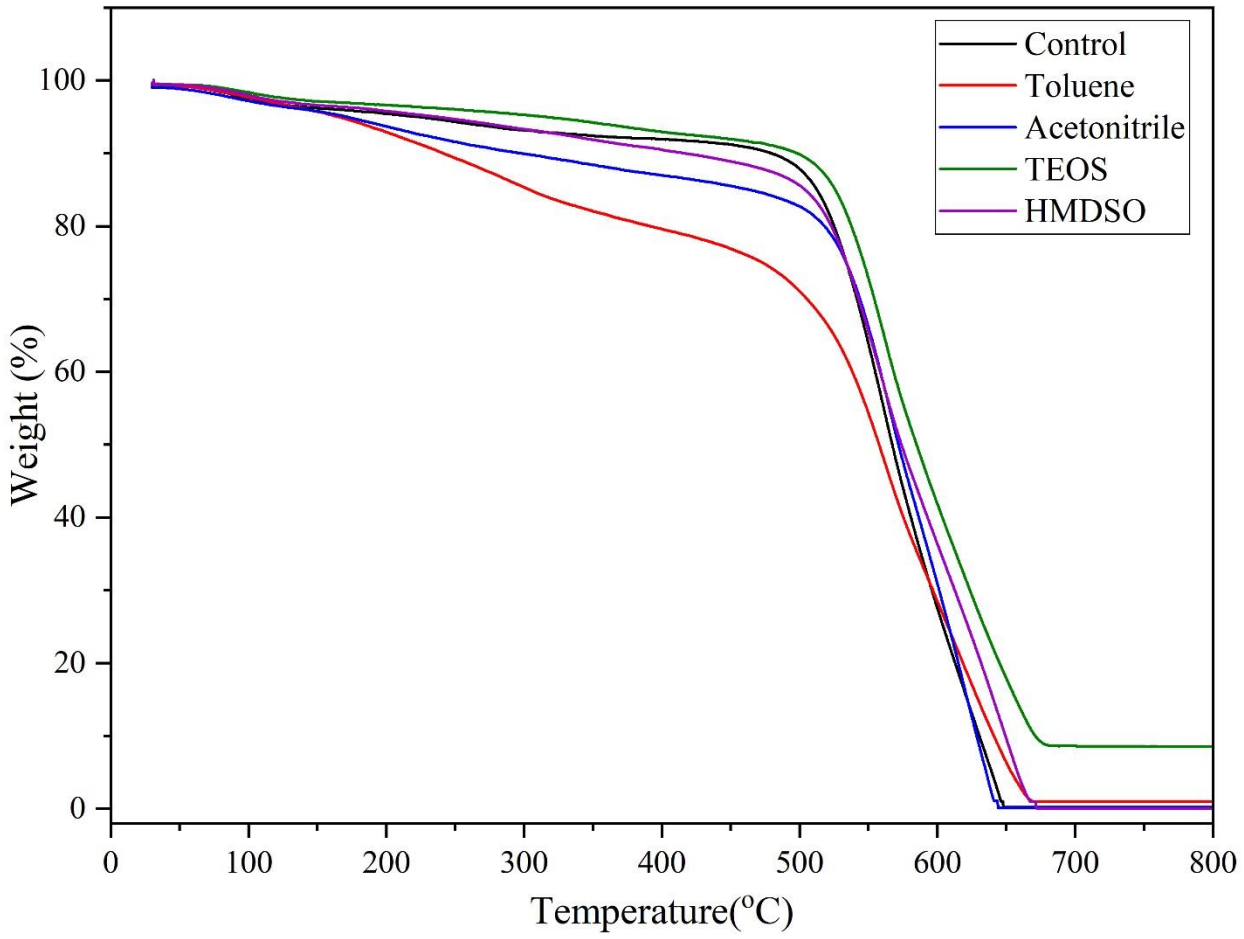


**Fig 10.** Thermal decomposition curves of uncoated and the plasma-coated fiber using with toluene, Acetonitrile, TEOS, HMDSO precursors

**Table 2.** Residual Percentage of uncoated and the plasma-coated fiber using with toluene, Acetonitrile, TEOS, HMDSO precursors in different temperatures

| Residual percentage (%) | 210 ºC | 400 ºC | 520 ºC | 800 ºC | Weigh loss between 0 to 800 ºC |
|---|---|---|---|---|---|
| Control | 95.24 | 91.92 | 82.23 | 0.23 | 99.77 |
| TEOS | 96.52 | 92.94 | 86.70 | 8.50 | 92.50 |
| HMDSO | 95.58 | 92.94 | 81.10 | 0.18 | 99.82 |
| Acetonitrile | 93.23 | 87.96 | 80.21 | 0.12 | 99.88 |
| Toluene | 92.23 | 79.61 | 66.50 | 1.00 | 99.00 |

### 3.3 Mechanical Properties

The effect of the plasma surface modification using different precursors on the breaking strength of the aramid fiber was investigated by tensile test. The results depict in Fig. 11 and the same breaking strength is observed for uncoated and plasma-coated aramid fibers using toluene, acetonitrile, and TEOS precursors. This suggests that no damage was induced on the aramid fibers by the plasma surface modification with these types of precursors and plasma apparatus. On the contrary, the plasma surface modifications with HMDSO precursors lead to an increase in the mechanical strength of the sample. This increment may be ascribed to the uniform deposition of Si groups on the surface of the aramid fibers followed by some deposition between adjacent fibers that leads to the interlinking of fibers (Figure S5).

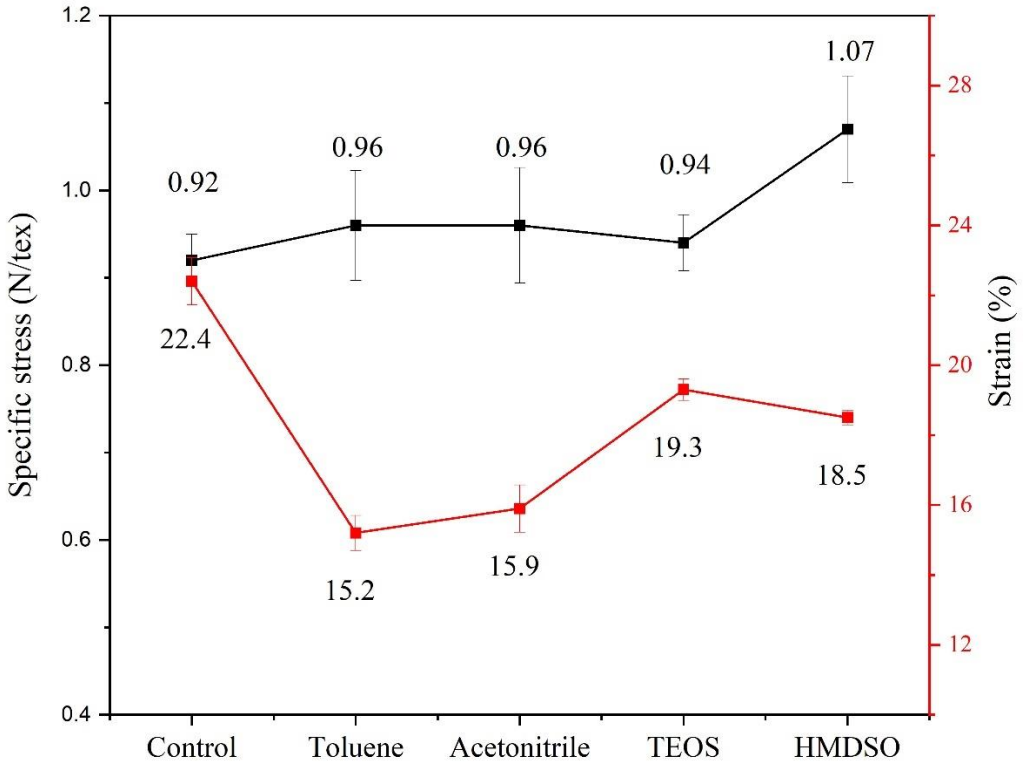


**Fig 11.** Specific Stress and strain curve of un coated and plasma- coated aramid fibers using toluene, acetonitrile, TEOS, and HMDSO

### 3.4 Interfacial adhesion of aramid/rubber composite

The pull-out test was performed to investigate the effects of the plasma treatments with different precursors on the interfacial adhesion of aramid/rubber composite. The results are depicted in Fig. 12. As can be seen from the results, by the plasma surface modification with hydrocarbon precursors including toluene and acetonitrile, we have an increment in aramid/rubber interfacial adhesion. The increment in interfacial adhesion aramid/rubber composite by DLC-based coating is maybe related to the generation of C=C bond on the surface of the aramid fibers, which directly chemical bond with the aramid and rubber matrix. Moreover, the formation of a nano-sphere particle on the surface of aramid fibers by plasma surface modification using hydrocarbon precursors (proved by FE-SEM analysis), increases the surface roughness followed by increment in surface area between aramid rubber that these two kinds of layers benefit the interfacial locking effect [52, 53].

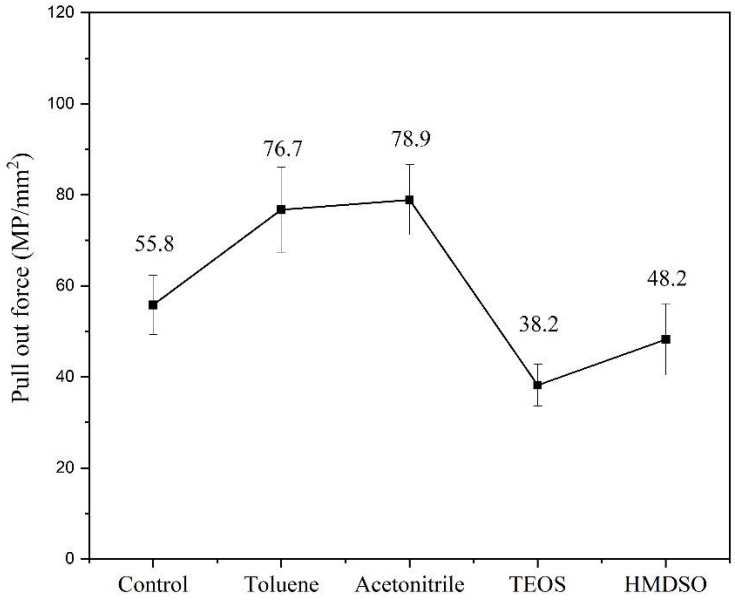


**Fig 12.** Pull out Force for uncoated and plasma-coated aramid fibers using toluene, acetonitrile, TEOS, and HMDSO

## 4. Discussion on results

Herein we briefed the results of some peer studies related to enhancing the adhesion effect between aramid fibers and rubber matrix with different methods in Table 4. As can be seen from the table, by comparing the results of this study with previous ones performed by a different method, it could be concluded that the atmospheric pressure plasma can be used as a promising method for enhancing the adhesion effect between aramid fibers and the rubber matrix.

**Table 8.** Briefed results of some peer studies related to enhance adhesion effect between aramid fibers and rubber matrix

| Author and publication data | Article title | Brief of the article | Pull out test |
|---|---|---|---|
| Current study | - | In the present study, the effect of the surface modification of aramid fibers using atmospheric pressure plasma treatment with different precursors on adhesion to the rubber matrix was investigated. For that, the plasma coating was conducted using argon as the main working gas, and toluene, acetonitrile, TEOS, and HMDSO as liquid precursors. | The results of the pull-out test show that the pull-out force between aramid fiber and rubber matrix was increased by 43% for plasma coated sample using acetonitrile precursor. |
| Zhang et al, 2022[54] | Mussel-inspired environmentally friendly dipping system for aramid fiber and its interfacial adhesive mechanism with rubber | In this study, a new dipping system was used for improving interfacial adhesion between aramid and rubber matrix. For this purpose, a network structure was prepared by water-soluble polyethyleneimine and pyrogallic acid and then | Based on the results of the pull-out test, the pull-out force between modified aramid fiber and rubber reached 147 N. The results show that the pull-out force |

| | | | |
|---|---|---|---|
| | | was mixed with rubber latex to prepare the dipping solution. | with this method is comparable with the level of a traditional resorcinol-formaldehyde-latex dipping system(154 N) while using harmful resorcinol and formaldehyde was avoided. |
| Yin et al, 2022[55] | Surface construction of ANF/CNT onto aramid fibers to enhance interfacial adhesion and provide real-time monitoring of deformation | In this study, functional groups such as hydroxyl and amino groups were introduced on the surface of aramid fiber by tannic acid and polyethyleneimine. Then, to prepare a surface-coated fiber, the modified aramid fiber was impregnated in the aramid nanofiber/carbon nanotube aqueous dispersion. | The results of this study shows that, compared to raw aramid fiber, the pull-out force of the coated one is increased by 126.4%. |
| Fang et al, 2022 [56] | Biomimetic surface modification of UHMWPE fibers to enhance interfacial adhesion with rubber matrix via constructing polydopamine functionalization platform and then depositing zinc oxide nanoparticles | In this study, a biomimetic surface modification method was used to enhance the interfacial adhesion between ultrahigh molecular weight polyethylene (UHMWPE) fibers and rubber matrix. The method consists of constructing a polydopamine functionalization platform and then depositing zinc oxide nanoparticles. | The results of the pull-out test show that the pull-out force of the UHMWPE and rubber matrix was increased to 34.3 N. This is equal to an 84.57% increase in interfacial adhesion between UHMWPE fibers and rubber matrix. |
| Zhang et al, 2021 [2] | Surface Coating of Aramid Fiber by a Graphene/Aramid Nanofiber Hybrid Material to Enhance Interfacial Adhesion with Rubber Matrix | In this study, a novel method of constructing nanostructures on the surface of aramid fiber through the $\pi$–$\pi^*$ interaction between the aramid nanofiber, graphene, and the graphene/aramid nanofiber dispersion in water. For this purpose, a layer was deposited on the surface of aramid fiber by immersion in an alkaline solution of tannic acid and polyethyleneimine, a tannic acid/polyethyleneimine. Then, the modified aramid fiber was impregnated with the graphene/aramid nanofiber dispersion to construct surface nanostructures on the surface of the aramid fiber. | The results of the pull-out test shows that the pull-out force of the aramid fiber and rubber matrix was increased by 84.7%, for the best sample. |
| Fang et al, 2021 [57] | Polydopamine and Mercapto Functionalized 3D Carbon Nano-Material Hybrids Synergistically Modifying Aramid Fibers for Adhesion Improvement | In this study, surface coating on the surface of aramid fiber was performed based on polydopamine, mercapto functionalized graphene oxide, and carbon nanotube. For that, firstly, graphene oxide, and carbon nanotube were assembled through $\pi$-$\pi$ conjugation. Then, the assembled graphene oxide/carbon nanotube hybrids were performed by dehydration condensation reaction between the hydroxyls of graphene oxide and the silanol groups of the coupling agent. Finally, the substance was grafted on the surface of aramid fibers. Also, before grafting the aramid fiber was modified by polydopamine. | The results of this study show that the pull-out force between coated aramid fiber and the rubber matrix was increased by 110.95% compared to the uncoated one. |

| | | | |
|---|---|---|---|
| Zhang et al, 2021[58] | Enhanced interfacial adhesion of aramid fiber reinforced rubber composites through bio-inspired surface modification and aramid nanofiber coating | In this study, at first, a surface coating on aramid fiber was performed with an alkaline solution of tannic acid and polyethyleneimine which led to the introduction of functional groups such as hydroxyl and amino groups on the surface of aramid fiber. Then, to improve the interfacial adhesion between the aramid fiber and the rubber, the cunstruction of nanostructure on the surface of modified aramid fiber was performed by an aramid nanofiber coating. | The results show that compared to raw aramid fiber, the interfacial adhesion of aramid fiber coated with aramid nanofiber was increased by 43.1% after 7 deposited cycles. Also, the results show that the mechanical properties of the fibers remain almost unchanged. |
| Zhang et al 2021 [59] | Nondestructive Grafting of ZnO on the Surface of Aramid Fibers Followed by Silane Grafting to Improve its Interfacial Adhesion Property with Rubber | In this study, a new method was used based on nondestructive grafting of zinc oxide onto a fiber surface followed by silane grafting. For this purpose, at first tannic acid and polyethyleneimine were used to form functional groups on the surface of aramid fibers. Then, by a hydrothermal reduction process, zinc oxide nanowires were deposited on the surface of modified aramid fibers. Finally, a polysulfide functionalized silane was grafted on the surface of the coated fiber. | The results of this study show that compared to uncoated aramid fiber, the interfacial adhesion between the modified fibers and rubber increased by 57%. Also, the results show that the breaking strength of aramid fibers does not change by the growth process of zinc oxide nanowires. |
| Yang et al, 2019 [5] | A Novel Method for Deposition of Multi-Walled Carbon Nanotubes onto Poly(p-Phenylene Terephthalamide) Fibers to Enhance Interfacial Adhesion with Rubber Matrix | In this study, a novel surface coating method was employed based on the deposition of multi-walled carbon nanotubes on the surface of PPTA to increase the interfacial adhesion between PPTA fiber and rubber matrix. The method was composed of the introduction of epoxy groups on the PPTA fibers, the carboxylation of MWCNTs, and the ring-opening reaction between the carboxyl and epoxy groups. | The results of this study shows that, compared to raw PPTA fiber, the pull-out force of the coated one is increased by 46.3%. |
| Wang et al, 2019 [7] | Enhanced adhesion property of aramid fibers by polyphenol-metal iron complexation and silane grafting | In this study, a green method has been used for surface coating on aramid fiber aiming to enhance their adhesion property with rubber matrix. For that, surface coating on aramid fiber was performed by polyphenol-metal by complexation between Fe(III) ions and tannic acid, followed by silane grafting. | The results of this study shows that, compared to raw aramid fiber, the pull-out force of the coated one is increased by 73.6%. |
| Yang et al, 2019 [60] | Surface modification of Poly(p-phenylene terephthalamide) fibers by polydopamine-polyethyleneimine/graphene oxide multilayer films to enhance interfacial adhesion with rubber matrix | In this study, a new surface coating method was employed based on graft polyethyleneimine-polydopamine/graphene oxide multilayer coating on the surface of PPTA fiber to increase the interfacial adhesion between PPTA fiber and rubber matrix. | The results of the pull-out test shows that the pull-out force of the aramid fiber and rubber matrix was increased by 78.1%, for the best sample. |
| Yang et al, 2019 [61] | Enhancing the interfacial adhesion with rubber matrix by grafting polydopamine-carbon nanotubes onto poly (p-phenylene terephthalamide) fibers | In this study, the interfacial adhesion between poly(p-phenylene terephthalamide) (PPTA) and rubber matrix was increased via aminated carbon nanotube deposition on the surface of PPTA fiber by combining the biomimetic modification of dopamine. | The results of this study shows that, compared to raw PPTA fiber, the pull-out force of the coated one is increased by 59.7%. |
| Kanbargi and Lesser 2017 [62] | Improving adhesion between aramid fibers and natural rubber through | In this article, a new method was employed to enhance the interfacial adhesion between PPTA fibers and natural rubber. For that, PPTA fiber | The results of this study shows that, compared to raw PPTA fiber, the pull-out |

| | | | |
|---|---|---|---|
| | morphological and synthetic modification of the fibers | underwent the pretreatment with two methods including a mechanical pretreatment and a microwave pretreatment. Then, the pretreated PPTA fibers were treated with coupling agents in the presence of supercritical carbon dioxide. | force of the coated one is increased by 100%. |
| Paolo et al, 2017 [63] | Microwave induced hierarchical nanostructures on aramid fibers and their influence on adhesion properties in a rubber matrix | In this study, a microwave-assisted surface modification of aramid fiber was used to improve adhesion between aramid fiber and rubber matrix. For that, the carbon evaporator method was employed to deposit a thin film of carbon onto the aramid fiber surface. Then microwave radiation was used to create hierarchical structures to the surface of aramid fiber. | The results of this study shows that, compared to raw aramid fiber, the bundle pull-out force of the coated one is increased by 259%. |
| Sa et al, 2015 [64] | Improved adhesion properties of poly-p-phenyleneterephthamide fibers with a rubber matrix via UV-initiated grafting modification | In this study, surface modification of PPTA was performed by ultraviolet irradiation-induced graft polymerization to enhance adhesion between PPTA fiber and rubber matrix. Also, resorcinol-formaldehyde–latex (REF) dipping was employed to further enhance in interfacial adhesion between PPTA fibers with the rubber matrix. | The results of this study show that, compared to raw PPTA fiber, the pull-out force of the coated one is increased by 53.7 % and 80.1% by grafted PPTA fibers and grafting PPTA fibers followed by RFL dipping respectively. |

## 5. Conclusion

In this study, the potential use of atmospheric pressure plasma for the production of aramid/rubber composites with promoted surface adhesion was investigated. For this purpose, a conventional atmospheric pressure plasma device was used to modify the surface of aramid fibers. For this purpose, argon was used as the main gas for the generation of plasma, and toluene, acetonitrile, TEOS, and HMDSO were used as liquid precursors. The surface modifications were performed under equal conditions for all samples.

Based on the results, the physical-chemical characterization of the aramid fibers before and after the plasma surface modifications confirmed the successful deposition of amorphous carbon, amorphous Nitride-carbon, $SiO_2$, and PDMS-like coating layers on the surface of aramid fibers by plasma surface modification using toluene, acetonitrile, TEOS, and HMDSO, respectively.

The pull-out test of coated aramid fiber indicated a 38%, and 43% increase in adhesion strength between toluene and acetonitrile aramid fiber and rubber materix respectively. The tensile test showed a 16% increase in the breaking strength of plasma-coated aramid fiber with HMDSO precursor, while no significant change was observed for plasma coating using toluene, acetonitrile, and TEOS precursors. The fire-retardancy test showed that the plasma-coated sample with HMDSO, and acetonitrile precursors, dose not any significantly different in weight loss at different

temperatures compared to uncoated fiber while for plasma coating with TEOS precursor, a 5.27% increase was detected.

So, the atmospheric plasma coating using acetonitrile precursors can be considered as a promising method for increasing adhesion between aramid fiber and rubber matrix for composite application. This method can lead to the promotion of interfacial adhesion of aramid/rubber while retaining the tensile strength, and flame resistance properties of aramid as original fibers. The method is simple, single-step, cost-effective, and environmentally friendly which has great potential for use in the rubber industry. Moreover, the operation is done at atmospheric pressure, which not only has no need for vacuum equipment but also has the potential for a continuous surface modification approach of aramid fiber.

## References


1. Afroughsabet, V., L. Biolzi, and T. Ozbakkaloglu, *High-performance fiber-reinforced concrete: a review.* Journal of materials science, 2016. **51**: p. 6517-6551.
2. Zhang, B., et al., *Surface coating of aramid fiber by a graphene/aramid nanofiber hybrid material to enhance interfacial adhesion with rubber matrix.* Industrial & Engineering Chemistry Research, 2021. **60**(6): p. 2472-2480.
3. Jia, C., et al., *Surface modification of aramid fibers by amino functionalized silane grafting to improve interfacial property of aramid fibers reinforced composite.* Polymer Composites, 2020. **41**(5): p. 2046-2053.
4. Liu, X.-D., et al., *UV-assisted surface modification of PET fiber for adhesion improvement.* Applied Surface Science, 2013. **264**: p. 61-69.
5. Yang, X., et al., *A novel method for deposition of multi-walled carbon nanotubes onto poly (p-phenylene terephthalamide) fibers to enhance interfacial adhesion with rubber matrix.* Polymers, 2019. **11**(2): p. 374.
6. Yang, X., et al., *Study on interfacial adhesion of the aramid fibers/rubber matrix by grafting mercapto hyperbranched polysiloxane.* Polymer Testing, 2020. **81**: p. 106259.
7. Wang, L., et al., *Enhanced adhesion property of aramid fibers by polyphenol-metal iron complexation and silane grafting.* The Journal of Adhesion, 2021. **97**(4): p. 346-360.
8. Wang, L., et al., *Surface modification of aramid fibers by catechol/polyamine codeposition followed by silane grafting for enhanced interfacial adhesion to rubber matrix.* Industrial & Engineering Chemistry Research, 2016. **55**(49): p. 12547-12556.
9. Wang, L., et al., *Highly efficient mussel-like inspired modification of aramid fibers by UV-accelerated catechol/polyamine deposition followed chemical grafting for high-performance polymer composites.* Chemical Engineering Journal, 2017. **314**: p. 583-593.
10. Lin, G., et al., *Combined treatments of fiber surface etching/silane-coupling for enhanced mechanical strength of aramid fiber-reinforced rubber blends.* Materials Chemistry and Physics, 2020. **255**: p. 123486.
11. Lin, J., et al., *Two-stage interface enhancement of aramid fiber composites: Establishment of hierarchical interphase with waterborne polyurethane sizing and oxazolidone-containing epoxy matrix.* Composites Science and Technology, 2020. **193**: p. 108114.
12. Chen, J., et al., *Surface modification and characterization of aramid fibers with hybrid coating.* Applied Surface Science, 2014. **321**: p. 103-108.
13. Loureiro, L., V.H. Carvalho, and S.H.P. Bettini, *Reuse of p-aramid from industrial waste as reinforcement fiber in polyamide 6.6.* Polymer Testing, 2016. **56**: p. 124-130.

14. Zhang, L., et al., *Supercritical CO2-induced nondestructive coordination between ZnO nanoparticles and aramid fiber with highly improved interfacial-adhesion properties and UV resistance.* Applied Surface Science, 2020. **521**: p. 146430.
15. Vedrtnam, A. and S.P. Sharma, *Study on the performance of different nano-species used for surface modification of carbon fiber for interface strengthening.* Composites Part A: Applied Science and Manufacturing, 2019. **125**: p. 105509.
16. Gore, P.M. and B. Kandasubramanian, *Functionalized aramid fibers and composites for protective applications: a review.* Industrial & Engineering Chemistry Research, 2018. **57**(49): p. 16537-16563.
17. Kang, H., T. Yoon, and W. Van Ooij, *Enhanced adhesion of aramid tire cords via argon plasma etching and acetylene plasma polymerization.* Journal of adhesion science and technology, 2006. **20**(11): p. 1155-1169.
18. de Lange, P.J. and P.G. Akker, *Adhesion activation of Twaron aramid fibers for application in rubber: Plasma versus chemical treatment.* Journal of adhesion science and technology, 2012. **26**(6): p. 827-839.
19. Li, S., et al., *Surface modification of aramid fibers via ammonia-plasma treatment.* Journal of Applied Polymer Science, 2014. **131**(10).
20. Zhang, B., et al., *Surface and interface modification of aramid fiber and its reinforcement for polymer composites: A review.* European Polymer Journal, 2021. **147**: p. 110352.
21. Gleissner, C., et al., *Surface activation of high performance polymer fibers: A review.* Polymer Reviews, 2022. **62**(4): p. 757-788.
22. Kale, K.H. and S.S. Palaskar, *Structural studies of plasma polymers obtained in pulsed dielectric barrier discharge of TEOS and HMDSO on nylon 66 fabrics.* Journal of the Textile Institute, 2012. **103**(10): p. 1088-1098.
23. Yuen, C., et al., *Influence of surface treatment on the electroless nickel plating of textile fabric.* Applied Surface Science, 2007. **253**(12): p. 5250-5257.
24. Elabid, A.E., et al., *Improving the low temperature dyeability of polyethylene terephthalate fabric with dispersive dyes by atmospheric pressure plasma discharge.* Applied Surface Science, 2016. **375**: p. 26-34.
25. Yu, H., et al., *Decomposition efficiency and aerosol by-products of toluene, ethyl acetate and acetone using dielectric barrier discharge technique.* Chemosphere, 2019. **237**: p. 124439.
26. PI, O.R.-U.F.A. and G. Gonzalez-Chi, *Deposition of carbon nanotubes onto aramid fibers using.* Surface and Coatings Technology, 2010. **204**: p. 3668-3675.
27. Xu, K., et al., *Preparation of robust aramid composite papers exhibiting water resistance by partial dissolution/regeneration welding.* Materials & Design, 2020. **187**: p. 108404.
28. JONGWANNASIRI, C. and S. WATANABE, *Effect of plasma treatment on friction coefficient of diamond-like carbon films.* Journal of The Surface Finishing Society of Japan, 2014. **65**(12): p. 621-624.
29. Cho, S.-J. and J.-H. Boo, *Characteristics of multilayered plasma-polymer thin films using toluene and TEOS by PECVD.* Microelectronic engineering, 2012. **89**: p. 19-22.
30. Rodil, S., *Infrared spectra of amorphous carbon based materials.* Diamond and related materials, 2005. **14**(8): p. 1262-1269.
31. Durand-Drouhin, O. and M. Benlahsen, *Internal stress of sputtered amorphous carbon nitride thin films.* Solid state communications, 2004. **131**(7): p. 425-429.
32. Goujon, M., T. Belmonte, and G. Henrion, *OES and FTIR diagnostics of HMDSO/O2 gas mixtures for SiOx deposition assisted by RF plasma.* Surface and Coatings Technology, 2004. **188**: p. 756-761.
33. Niu, J., et al., *Growth, structure, and mechanical properties of hydrogenated amorphous carbon nitride films deposited by CH3CN dielectric barrier discharges.* Journal of Applied Physics, 2010. **107**(6).

34. Nowling, G., et al., *Chamberless plasma deposition of glass coatings on plastic.* Plasma Sources Science and Technology, 2005. **14**(3): p. 477.
35. Lo, C.-H., et al., *Plasma deposition of tetraethoxysilane on polycarbonate membrane for pervaporation of tetrafluoropropanol aqueous solution.* Journal of Membrane Science, 2009. **329**(1-2): p. 138-145.
36. Abbasi-Firouzjah, M., et al., *The effect of TEOS plasma parameters on the silicon dioxide deposition mechanisms.* Journal of Non-Crystalline Solids, 2013. **368**: p. 86-92.
37. Hilt, F., et al., *Efficient flame retardant thin films synthesized by atmospheric pressure PECVD through the high co-deposition rate of hexamethyldisiloxane and triethylphosphate on polycarbonate and polyamide-6 substrates.* ACS Applied Materials & Interfaces, 2016. **8**(19): p. 12422-12433.
38. Maurau, R., et al., *Nitrogen Introduction in pp-HMDSO Thin Films Deposited by Atmospheric Pressure Dielectric Barrier Discharge: An XPS Study.* Plasma Processes and Polymers, 2012. **9**(3): p. 316-323.
39. Atanasov, S.E., et al., *Improved cut-resistance of Kevlar® using controlled interface reactions during atomic layer deposition of ultrathin (< 50 Å) inorganic coatings.* Journal of Materials Chemistry A, 2014. **2**(41): p. 17371-17379.
40. Dong, L., et al., *Surface construction of fluorinated TiO 2 nanotube networks to develop uvioresistant superhydrophobic aramid fabric.* RSC advances, 2020. **10**(38): p. 22578-22585.
41. Zeng, L., et al., *Surface modification of aramid fibres with graphene oxide for interface improvement in composites.* Applied Composite Materials, 2018. **25**: p. 843-852.
42. Shiju, J., F. Al-Sagheer, and Z. Ahmad, *Thermal mechanical properties of graphene nano-composites with Kevlar-Nomex copolymer: A comparison of the physical and chemical interactions.* Polymers, 2020. **12**(11): p. 2740.
43. Kanerva, M., et al., *DLC-treated aramid-fibre composites: Tailoring nanoscale-coating for macroscale performance.* Composites Science and Technology, 2019. **171**: p. 62-69.
44. Nakao, S., et al., *Characterization of diamond-like carbon films prepared using various source gases by plasma-based ion implantation and deposition.* Surface and Coatings Technology, 2018. **355**: p. 136-142.
45. Fang, T., et al., *The effect of the H2/(H2+ Ar) flow-rate ratio on hydrogenated amorphous carbon films grown using Ar/H2/C7H8 plasma chemical vapor deposition.* Thin Solid Films, 2018. **660**: p. 891-898.
46. Derudi, M., D. Polino, and C. Cavallotti, *Toluene and benzyl decomposition mechanisms: elementary reactions and kinetic simulations.* Physical Chemistry Chemical Physics, 2011. **13**(48): p. 21308-21318.
47. Liang, W., et al., *Abatement of toluene from gas streams via ferro-electric packed bed dielectric barrier discharge plasma.* Journal of hazardous materials, 2009. **170**(2-3): p. 633-638.
48. Fracassi, F., R. d'Agostino, and P. Favia, *Plasma-enhanced chemical vapor deposition of organosilicon thin films from tetraethoxysilane-oxygen feeds.* Journal of the Electrochemical Society, 1992. **139**(9): p. 2636.
49. Arolkar, G.A., et al., *Effect of TEOS plasma polymerization on corn starch/poly (3-caprolactone) film: characterization, properties and biodegradation.*
50. Boscher, N.D., et al., *Chemical compositions of organosilicon thin films deposited on aluminium foil by atmospheric pressure dielectric barrier discharge and their electrochemical behaviour.* Surface and Coatings Technology, 2010. **205**(7): p. 2438-2448.
51. Zhang, M.-M., et al., *Hyperbranched polysiloxane functionalization of graphene oxide for improved mechanical properties of cyanate ester nanocomposites.* Journal of Composite Materials, 2015. **49**(8): p. 939-948.
52. Cheng, Z., et al., *Aramid fiber with excellent interfacial properties suitable for resin composite in a wide polarity range.* Chemical Engineering Journal, 2018. **347**: p. 483-492.

53. Karl, C.W., et al., *Surface modification of ethylene propylene diene terpolymer rubber by plasma polymerization using organosilicon precursors.* ACS Applied Polymer Materials, 2020. **2**(9): p. 3789-3796.
54. Zhang, B., et al., *Mussel-inspired environmentally friendly dipping system for aramid fiber and its interfacial adhesive mechanism with rubber.* Polymer, 2022. **238**: p. 124414.
55. Li, T., et al., *Non-destructive modification of aramid fiber by building nanoscale-coating solution to enhance the interfacial adhesion properties of the fiber-reinforced composites.* Journal of Composite Materials, 2021. **55**(13): p. 1823-1834.
56. Fang, Z., et al., *Biomimetic surface modification of UHMWPE fibers to enhance interfacial adhesion with rubber matrix via constructing polydopamine functionalization platform and then depositing zinc oxide nanoparticles.* Surfaces and Interfaces, 2022. **29**: p. 101728.
57. Fang, Z., et al., *Polydopamine and Mercapto Functionalized 3D Carbon Nano-Material Hybrids Synergistically Modifying Aramid Fibers for Adhesion Improvement.* Polymers, 2022. **14**(19): p. 3988.
58. Zhang, B., et al., *Enhanced interfacial adhesion of aramid fiber reinforced rubber composites through bio-inspired surface modification and aramid nanofiber coating.* Journal of Applied Polymer Science, 2021. **138**(39): p. 51011.
59. Zhang, B., et al., *Nondestructive grafting of ZnO on the surface of aramid fibers followed by silane grafting to improve its interfacial adhesion property with rubber.* ACS Applied Polymer Materials, 2021. **3**(9): p. 4587-4594.
60. Yang, X., et al., *Surface modification of Poly (p-phenylene terephthalamide) fibers by polydopamine-polyethyleneimine/graphene oxide multilayer films to enhance interfacial adhesion with rubber matrix.* Polymer Testing, 2019. **78**: p. 105985.
61. Yang, X., et al., *Enhancing the interfacial adhesion with rubber matrix by grafting polydopamine-carbon nanotubes onto poly (p-phenylene terephthalamide) fibers.* Polymers, 2019. **11**(8): p. 1231.
62. Kanbargi, N. and A.J. Lesser, *Improving adhesion between aramid fibers and natural rubber through morphological and synthetic modification of the fibers.* Journal of Applied Polymer Science, 2018. **135**(24): p. 45520.
63. Palola, S., et al., *Microwave induced hierarchical nanostructures on aramid fibers and their influence on adhesion properties in a rubber matrix.* Applied Surface Science, 2017. **410**: p. 145-153.
64. Sa, R., et al., *Improved adhesion properties of poly-p-phenyleneterephthamide fibers with a rubber matrix via UV-initiated grafting modification.* RSC advances, 2015. **5**(114): p. 94351-94360.